# ResearchOnline@JCU



This is the author-created version of the following work:

Kamel, Michael S.A., Oelgemöller, Michael, and Jacob, Mohan V. (2022) Sustainable plasma polymer encapsulation materials for organic solar cells. Journal of Materials Chemistry A, 10 (9) pp. 4683-4694.

Access to this file is available from:

https://researchonline.jcu.edu.au/72998/

This journal is © The Royal Society of Chemistry 2022.

Please refer to the original source for the final version of this work:

https://doi.org/10.1039/d1ta10608b

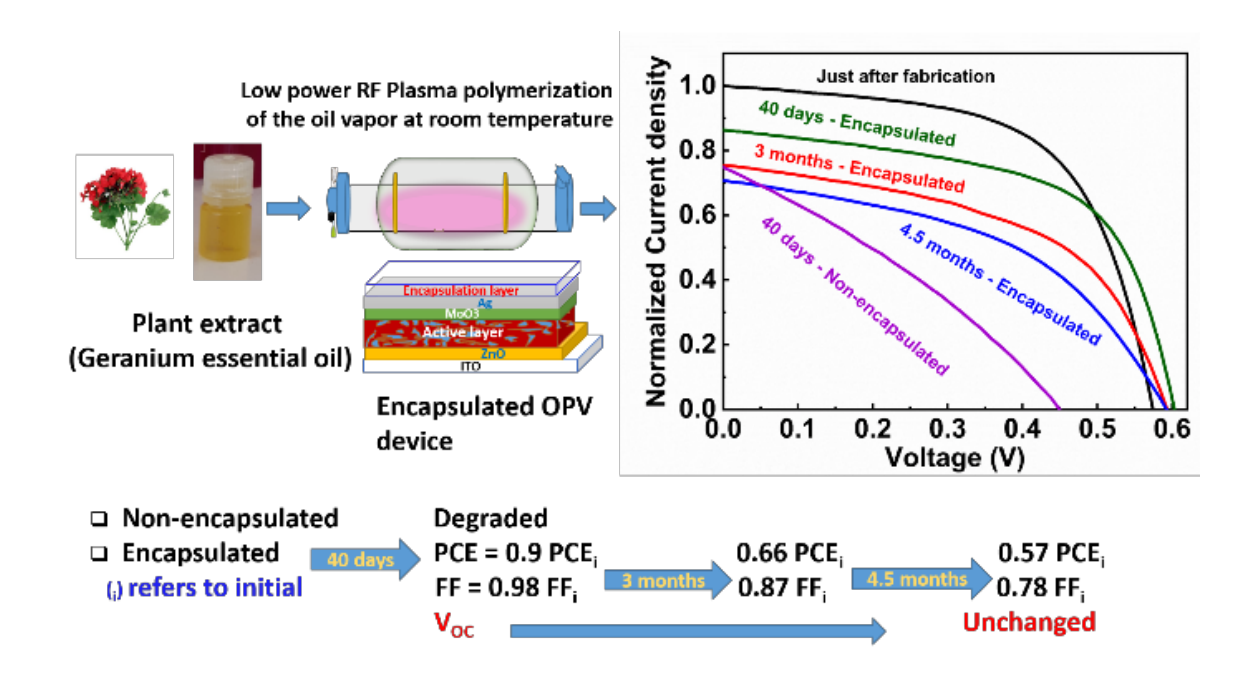
## Sustainable plasma polymer encapsulation materials for organic solar cells

Michael S. A. Kamel ab, Michael Oelgemöller and Mohan V. Jacob a

<sup>a</sup> Electronic Materials Research Lab, College of Science and Engineering, James Cook University,

Townsville 4811, Australia

The rapid degradation of organic photovoltaics (OPVs) under ambient conditions represents a major limitation to this promising technology. Device encapsulation is an effective approach to increase the lifetime of OPVs. Herein, we report the time and cost-effective synthesis of ultrathin encapsulation materials for OPVs by radio frequency (RF) plasma polymerization from plant extract. The encapsulated device retained 66% and 87% of its initial power conversion efficiency (PCE) and fill factor, respectively, after 90 days in ambient conditions while the reference device degraded within the first month. More interestingly, the open circuit voltage of the encapsulated device was found unchanged after > 4.5 months with 70 % of its original short circuit current density. The investigated thin films have shown strong absorption in the ultraviolet (UV) range with high transmission exceeding 98% to visible light which can employed to prevent harmful UV photons from reaching the photoactive layer of the device. Additionally, the synthesized films have revealed a high chemical stability under artificial UV irradiation. Thus, this work presents a solvent-free and room temperature encapsulation method from sustainable materials to increase the lifetime of OPVs without altering the device performance.



#### **Contents**

1. Introduction

<sup>&</sup>lt;sup>b</sup> Physics Department, Faculty of Science, Minia University, P.O. Box 61519 Minia, Egypt

<sup>&</sup>lt;sup>c</sup> Applied and Green Photochemistry Group, College of Science and Engineering, James Cook University, Townsville 4811, Australia

2. Fabrication and characterization methods	3
2.1 Device fabrication	3
2.2 Device encapsulation	4
2.3 Device stability measurements	5
2.4 Characterization of PP-thin films	5
3. Results and discussions	5
3.1 Photovoltaic stability of the encapsulated OPVs	5
3.2 Morphology and surface homogeneity of plasma polymerized thin films	8
3.3 Optical properties of PP-thin films	10
3.4 Chemical structure and photostability of PP-thin films	12
3.5 Water contact angle of PP-thin films	15
4. Conclusion	16
Conflicts of interest	16
Acknowledgement	16
References	17

## 1. Introduction

Organic solar cells (OSCs) have received intensive research attention over the past decade as a promising alternative to their high cost inorganic based counterparts <sup>1-3</sup>. The mechanical flexibility <sup>4, 5</sup>, low processing cost <sup>6, 7</sup>, light-weight <sup>8, 9</sup>, abundance of materials and rapidly increasing power conversion efficiency (PCE) represent the major advantages of OSCs <sup>10, 11</sup>. The PCE of organic photovoltaics (OPVs) has jumped from approximately 7% <sup>12</sup> to >18% for monolayer <sup>13, 14</sup>, <sup>15, 16</sup> and exceeding 17% for multi-layer tandem devices <sup>17, 18</sup> since 2010. However, the short lifetime of OPVs under real world operating conditions hinders their large-scale commercialization. Typical lifetimes of OPVs range from a few to thousands of hours in air <sup>19</sup>. However, these lifetimes increase significantly when devices are stored in inert atmosphere <sup>20</sup>. The prolonged exposure of OPVs to oxygen, water vapour, temperature, and ultraviolet (UV) light stimulates oxidation reactions at the interface between, and within, the different layers of the device. These reactions result in compositional changes which eventually lead to the degradation of the photovoltaic parameters and overall device performance <sup>19, 21, 22</sup>.

Different approaches were proposed to reduce the degradation of OPVs such as the development of inverted geometry which allowed the utilization of metal electrodes with high work functions such as Silver (Ag) and Gold (Au). The high work function electrodes show higher resistance to the photo-oxidation reactions under real world conditions compared to Aluminium cathode in case of regular geometry OPVs <sup>23, 24</sup>. Additionally, inverted geometry stopped the degradation of the ITO transparent electrode caused by the acidic nature of the most commonly used hole transport layer (HTL) poly(3,4-ethylenedioxythiophene) polystyrene sulfonate (PEDOT:PSS) <sup>25, 26</sup>. Despite the performance improvement achieved with the inverted OPVs the long-term operation under ambient conditions

eventually results in device degradation. Therefore, physical encapsulation of OPVs is an essential procedure to increase their lifetimes through reducing the amount of oxygen and water vapour reaching the different layers of the device <sup>19, 27</sup>. The utilization of glass-based encapsulation prevents the application of flexible OPVs. Several attempts were reported to synthesize efficient encapsulation materials for flexible electronic devices including plastic and graphene-based barriers <sup>28-31</sup>. However, these methods are based on multi-step processes and/ or require additional adhesive (sealing) materials and further UV treatment to adhere to the encapsulated device.

An effective encapsulation material should possess low water and oxygen permeability, high resistance to thermal and UV degradation, and high electric permittivity. Moreover, good adhesion to the device to be encapsulated and low cost processability are of great importance  $^{27,32}$ . Plant extract-based radio frequency (RF) plasma polymers (PPs) offer outstanding features such as their sustainable generation, stability, chemical inertness, mechanical flexibility, defect-free structure, high optical transparency, and time and cost effective and solvent-free processing  $^{33-36}$ . Plant extracts-derived RF PPs are promising candidates as encapsulation materials for OPVs and other optoelectronic devices especially for flexible applications. Many reports have referred to the potential of PPs from essential oils as encapsulation layers for electronic devices  $^{37-39}$ . However, only one attempt has been made to encapsulate OPVs with such thin film polymers where  $\gamma$ -terpinene PP based on continuous RF plasma was employed  $^{33}$ . The properties of the synthesized PP-thin films can vary widely with the preparation conditions such as the power and the mode of RF plasma, deposition time, monomer type and flow rate, etc. More research is needed to develop new encapsulation materials and to investigate any potential applications of these sustainable and low cost PPs in OPVs and other optoelectronic devices.

In this work, Pelargonium graveolens (geranium oil) was used to produce plasma polymerized thin films, by both continuous and pulsed RF plasma. Thin film coatings were synthesized directly on the top of the metal electrode of inverted geometry P3HT: PCBM based OPV devices. The effect of RF power and duty cycle (D.C) in case of continuous and pulsed plasma, respectively, on the film properties as well as device stability was investigated. The stability of the encapsulated and non-encapsulated OPVs against ambient conditions was investigated via measuring the current density-voltage (J-V) characteristics over three months. The variation of the photovoltaic parameters; short circuit current density ( $J_{SC}$ ), open circuit voltage ( $V_{OC}$ ), fill factor (FF), and power conversion efficiency (PCE) of the devices with time was investigated. Different techniques such as FTIR, AFM, water contact angle, UV-VIS and Ellipsometer were used to characterize the synthesized PP thin films. Moreover, the photo-stability the prepared PP-thin films was studied under ultraviolet (UV) irradiation.

## 2. Fabrication and characterization methods

## 2.1 Device fabrication

Inverted geometry bulk heterojunction (BHJ) OPV devices with structure ITO/ZnO/P3HT: PCBM/MoO<sub>3</sub>/Ag were employed in the present study (Fig. 1a). Pre-patterned (20 mm x 15 mm) ITO-coated glass substrates (S211) purchased from Ossila were cleaned in ultrasonic bath of DI water with decon-90, DI water, acetone and isopropyl alcohol (IPA) subsequently for 10 minutes each. The cleaned substrates were then dried by air gun and left overnight in an oven at  $100^{\circ}$ C to remove any residual water or solvents. Finally, the dried substrates were exposed to 50 W O<sub>2</sub> plasma for 20 minutes for surface modification just before the deposition of ZnO electron transport layer (ETL). To produce ZnO sol-gel, 0.109 g of Zn-Acetate dihydrate was dissolved in 1 ml of 2-methoxyethanol (Purity > 99%) with 32  $\mu$ l of ethanolamine (Purity > 99.5 %) as a stabilizer. All the components of ZnO sol-gel were obtained from Sigma Aldrich. ZnO Solution was stirred at 60°C for two hours followed by overnight rigorous stirring at room temperature. The clear ZnO sol-gel was then filtered using 0.45  $\mu$ m PTFE hydrophobic filters before spin coating to exclude any agglomerations. To get a thin (~30 nm)

ETL of ZnO, 40  $\mu$ l of the solution was spin coated at 4000 rpm for 60 seconds on the top of ITO, then annealed on a hotplate at 170°C for 30 minutes in open air <sup>40,41</sup>. After that, the coated substrates were moved to a Nitrogen-filled glovebox for the deposition of the photoactive layer through the spin coating of 20  $\mu$ l of the P3HT: PCBM (1:0.8 weight ratio) dissolved in chlorobenzene with total concentration of 25 mg/ml on the top of ZnO layer at 2000 rpm for 35 seconds followed by 10 minutes annealing on hotplate at 120°C. For the deposition of the top electrode (anode), the substrates were then transferred to thermal evaporation unit (Model: HINDI HIVACUUM 12A4D). A thin layer (~ 2.3 nm) of MoO<sub>3</sub> HTL, then 100 nm of Ag (anode) were evaporated under high vacuum of 5 ×10<sup>-6</sup> mbar. The active area of each single device was decided by the deposition mask (S211 from Ossila) to be 4 mm². Eight devices were fabricated for each type under investigation. After the deposition of the anode, devices were moved directly to the RF plasma reactor for encapsulation.

## 2.2 Device encapsulation

A thin layer of plasma-polymerized Pelargonium graveolens was deposited on the top of the metal electrode using a custom-made plasma polymerization system as shown in Fig. 1b. Pelargonium graveolens was obtained from Australian botanical products and was used without further treatments. The major constituents of the precursor are citronellol (34.12%), geraniol (13.69%), citronellyl formate (7.39%), isomenthone (5.74%), and linalool (5.19%). The RF plasma polymerization reactor consists of a 70 cm long quartz tube (with inner diameter = 5 cm) connected to a vacuum pump at one end and to the precursor inlet at the other side. Two copper rings were mounted around the tube and fixed 10 cm apart. The output terminals of an RF generator (CESAR 1312 RF power generator) with frequency of 13.56 MHz were connected to the copper rings through matching network (Navio RF matching network – Advanced Energy -M/N 3155401-002 C). The OPV devices to be encapsulated were inserted into the tube at between the Cu electrodes. The tube was evacuated at a pressure of (0.1-0.2) mbar before the monomer vapour was released to enter the reactor. For continuous plasma, different RF power levels (10, 15, 20, 25, and 30 W) were applied for 10 minutes to produce the plasma polymerized encapsulation layers. On the other hand, 30 W of pulsed power was applied at three different duty cycles (30%, 50%, and 70%) while all other conditions were kept the same as continuous plasma. Tiny pieces of sticky tape were used to cover the end sides of the ITO stripes to avoid blocking the device terminals with the encapsulation film. Both encapsulated and nonencapsulated devices were then stored in ambient conditions to investigate their stability. For air stability investigation, devices were stored in ambient conditions, outside the glovebox. The stability of the devices was investigated by studying their J-V curves over 2160 hours.

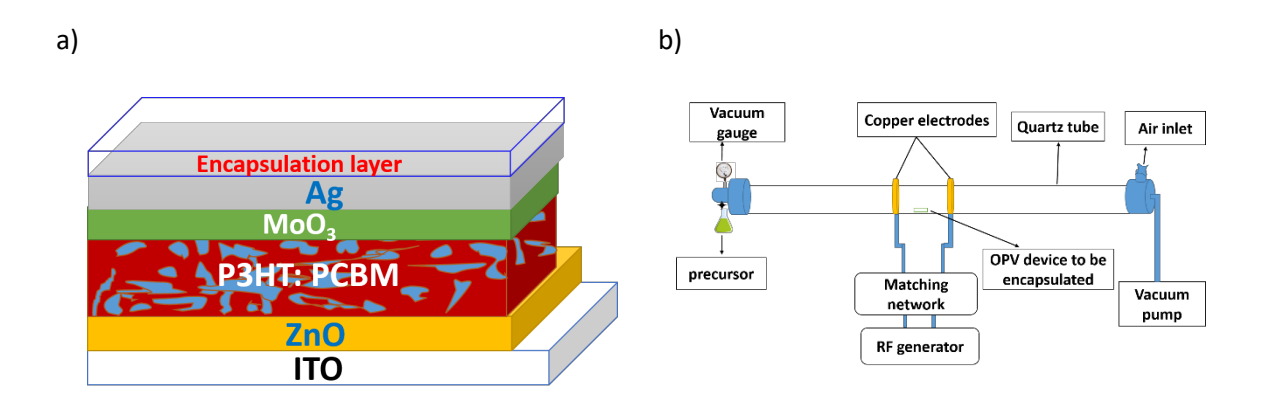


**Fig. 1 (a)** Inverted structure BHJ OPV device with encapsulation layer, b) experimental setup for the RF plasma polymerization reactor.

#### 2.3 Device stability measurements

The stability of the as-fabricated (reference) and encapsulated OPVs against ambient air was investigated over three months. However, the top device based on pulsed plasma encapsulation was tested once again after extra 1.5 months i.e. a total of 4.5 months. The variation of the photovoltaic parameters e.g.  $J_{SC}$ ,  $V_{OC}$ , FF, and PCE of the devices stored in ambient atmosphere was studied as a function of time. The performance of the investigated devices was obtained by studying their J-V characteristics under one sun illumination of AM1.5G solar simulator (ABET Sunlite) with 100 mW/cm² incident illumination. The solar simulator was calibrated before the J-V measurements using a standard Si solar cell as a reference. J-V curves were recorded with the help of Keithley 2636A source meter and E370 test board (from Ossila).

#### 2.4 Characterization of PP-thin films

The chemical structure of the prepared plasma polymers at different deposition power levels was studied using ATR FTIR (PerkinElmer Spectrum 100 FTIR spectrometer). Moreover, the photostability of the investigated encapsulation PP-thin films was also studied by studying the change in their FTIR spectra as a result of exposure to UV radiation. Variable angle spectroscopic Ellipsometer (J.A. Woollam Co. Inc. M-2000D) was used to study the thickness of the as fabricated films via the analysis of the reflection and transmission spectra with the help of CompleteEASE 6.56 software. Optical constants such as refractive index and attenuation coefficient were also studied. Moreover, the UV absorption and optical bandgap of the different plasma polymerized thin films were investigated using UV-VIS spectrometer (Shimatzu UV-VIS 2600) with wavelength range of 200 to 800 nm. Goniometer instrument (KSV CAM 101, Helsinki, Finland) was used to investigate the wetting properties of the PPfilms through studying the water contact angle. Morphology of the prepared films was studied using atomic force microscope (AFM) (NT-MDT NTEGRA, Moscow, Russian). The stability of the synthesized pp-films under UV irradiation was studied using a photoreactor chamber (Luzchem LZC-1). The reactor consists of a top illuminated chamber with eight 8 W UVB lamps (Ushio G8T5E; wavelength range 300  $\pm$  25 nm). The chamber had dimensions of 33  $\times$  33 cm (L  $\times$  W) and 22 cm (H). The film temperature during irradiation was kept at almost ± 3°C from room temperature with the help of the exhaust fan at the back of the chamber. The stability of the films under UV irradiation was investigated by studying the variation of their FTIR spectra with UV doses.

### 3. Results and discussions

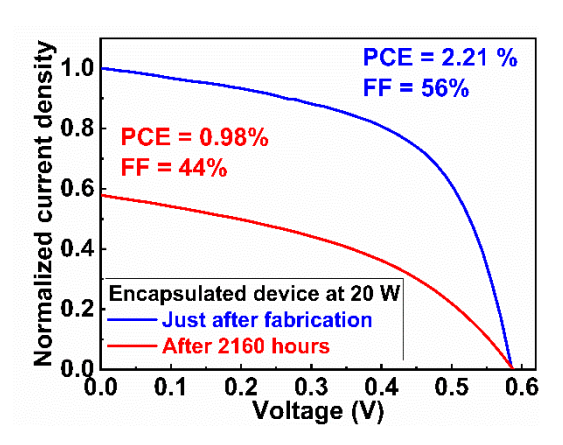
#### 3.1 Photovoltaic stability of the encapsulated OPVs

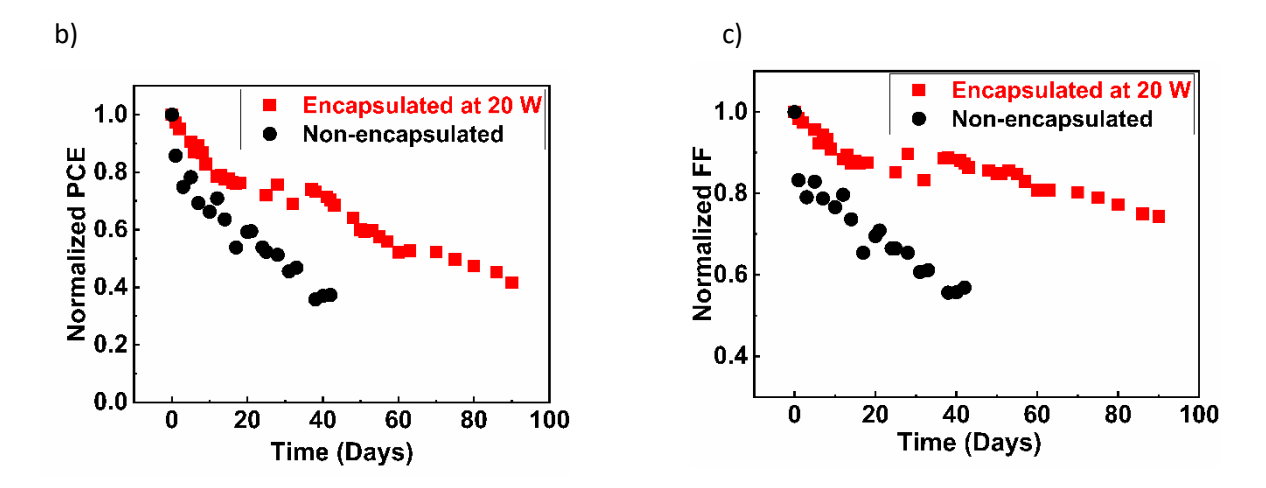
Fig. 2 shows the performance variation of OPV devices both encapsulated with PP-thin film deposited at 20 W RF continuous plasma (CP) and non-encapsulated as a function of time. In Fig. 2a the variation of the J-V curves of the reference device as well as devices encapsulated at 20 W RF CP after fabrication and after 2160 hours. The performance of the reference device completely deteriorated in comparison with the encapsulated counterparts, which retained almost 50% of their initial performance after 2160 hours. The value of open circuit voltage of the devices encapsulated at 20 power also remained unchanged even after three months in ambient conditions. The decay of the photovoltaic performance of the encapsulated devices is mainly attributed to the reduction  $J_{SC}$  unlike the reference device, which showed high loss in both  $J_{SC}$  and  $V_{OC}$ . The simultaneous decrease in  $V_{OC}$  and  $J_{SC}$  for the non-encapsulated device may be an evidence for dramatically reduced  $R_{Sh}$  and increased  $R_{Sh}$  of the device. On the other hand, the highly stable  $V_{OC}$  of encapsulated devices confirms that their shunt resistance has not or only slightly changed over >2100 hours, while the drop on their  $J_{SC}$  is attributed to  $R_{Sh}$  increase. The increased  $R_{Sh}$  is attributed to the increased resistance of the metal electrode upon oxidation in the ambient atmosphere. It is worth mentioning that water and oxygen

molecules not only diffuse through the device during its lifetime, but can also be captured during device fabrication <sup>19</sup>. Thus, part of the performance degradation of the investigated devices can be attributed to the presence of O<sub>2</sub> and H<sub>2</sub>O molecules within the fabrication steps in particular during the metal electrode deposition and encapsulation which were conducted outside the glovebox. Therefore, the integration of these steps with the glovebox is expected to significantly increase the device lifetime.

For pulsed plasma-based encapsulation layers, the variation of device performance with time showed higher stability compared to those based on continuous plasma. From Fig. 3, OPVs encapsulated with pulsed PP-thin films have retained almost 90% of their initial PCE and ~95% of both J<sub>SC</sub> and FF during the first 25 days (600 h). In the following 20 days (after 1080 hours), the encapsulated devices have revealed high performance with keeping more than 83% and >92% of their PCEs and FFs, respectively, compared to the reference counterpart that lost almost 60% of its initial PCE after almost 900 hours. The stability of the devices encapsulated at DC of 30% and 50% have higher stability than those encapsulated at DC of 70%. After 2160 hours (90 days), OPVs encapsulated at DC 30% and 50% retained 66% and 67% and 82% and 83% of their initial PCEs and fill factors, respectively. At higher DC (70%), the device retained 61% and 75% of its original PCE and FF, respectively, after three months. The remaining J<sub>SC</sub> decreased from 78% to 74% with increasing DC from 30% to 50% and then to 72% at DC of 70%. Additionally, the value of V<sub>OC</sub> for all the encapsulated devices have shown no change over the investigated time (90 days). More interestingly, the device encapsulated at DC of 50% was found to retain > 57% and 78% of its original PCE and FF, respectively, without any loss in its V<sub>OC</sub> even after 3264 hours (136 days) as shown in Fig. 3a. These values recorded after 4.5 months are still higher than those obtained with the reference device after less than three weeks. The obtained results confirm that OPVs encapsulated with geranium oil-based pulsed plasma polymers have higher stability than the continuous plasma based counterparts either synthesized from geranium oil, in the present work, or from  $\gamma$ -terpinene in ref.<sup>33</sup>. The addition of PP coating on the top electrode of the OPV device plays a significant role in improving device stability. The presence of encapsulation films on the top of the metal electrode limits the passage of O<sub>2</sub> and water vapour, which leads to fast degradation, through the different layers of the device. Therefore, the photo-induced oxidation reactions at the interfaces as well as the metal electrode are slowed down and hence higher stability is achieved.

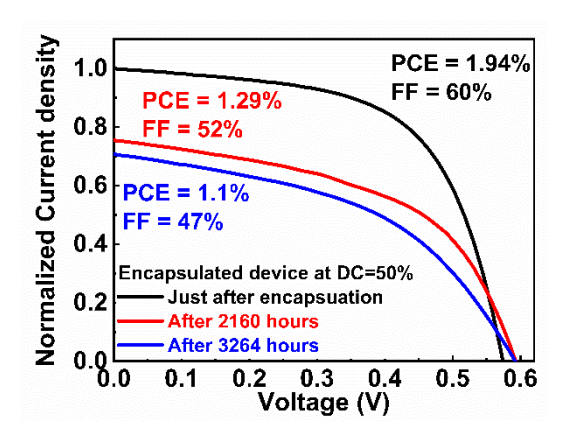
a)

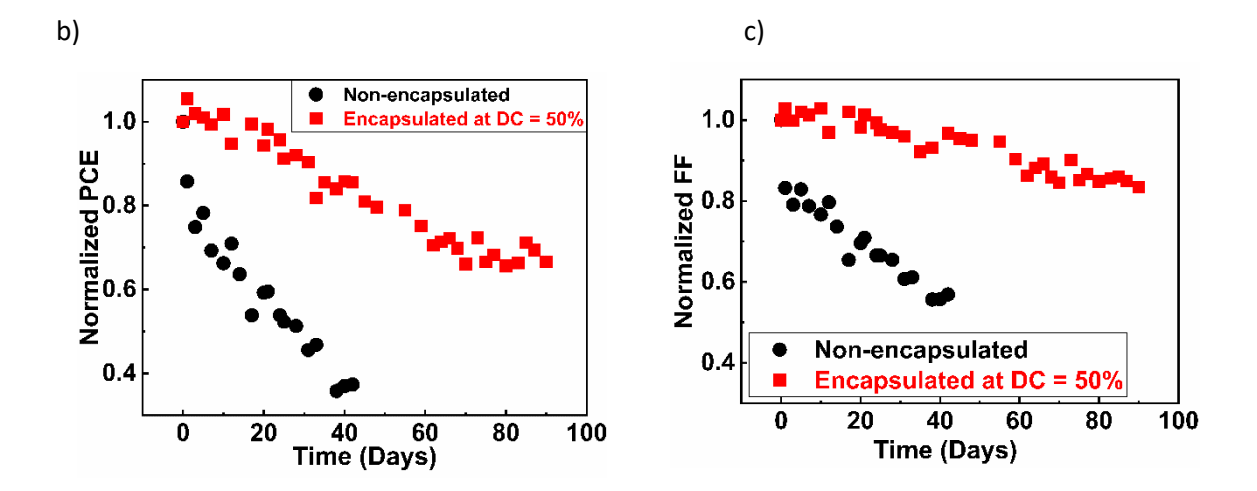




**Fig. 2** (a) Normalized J-V characteristics of encapsulated device with continuous plasma of 20 W RF after fabrication and 2160 hours outside the glovebox. The variation of PCE b) and FF c) with time for encapsulated and non-encapsulated device.

a)





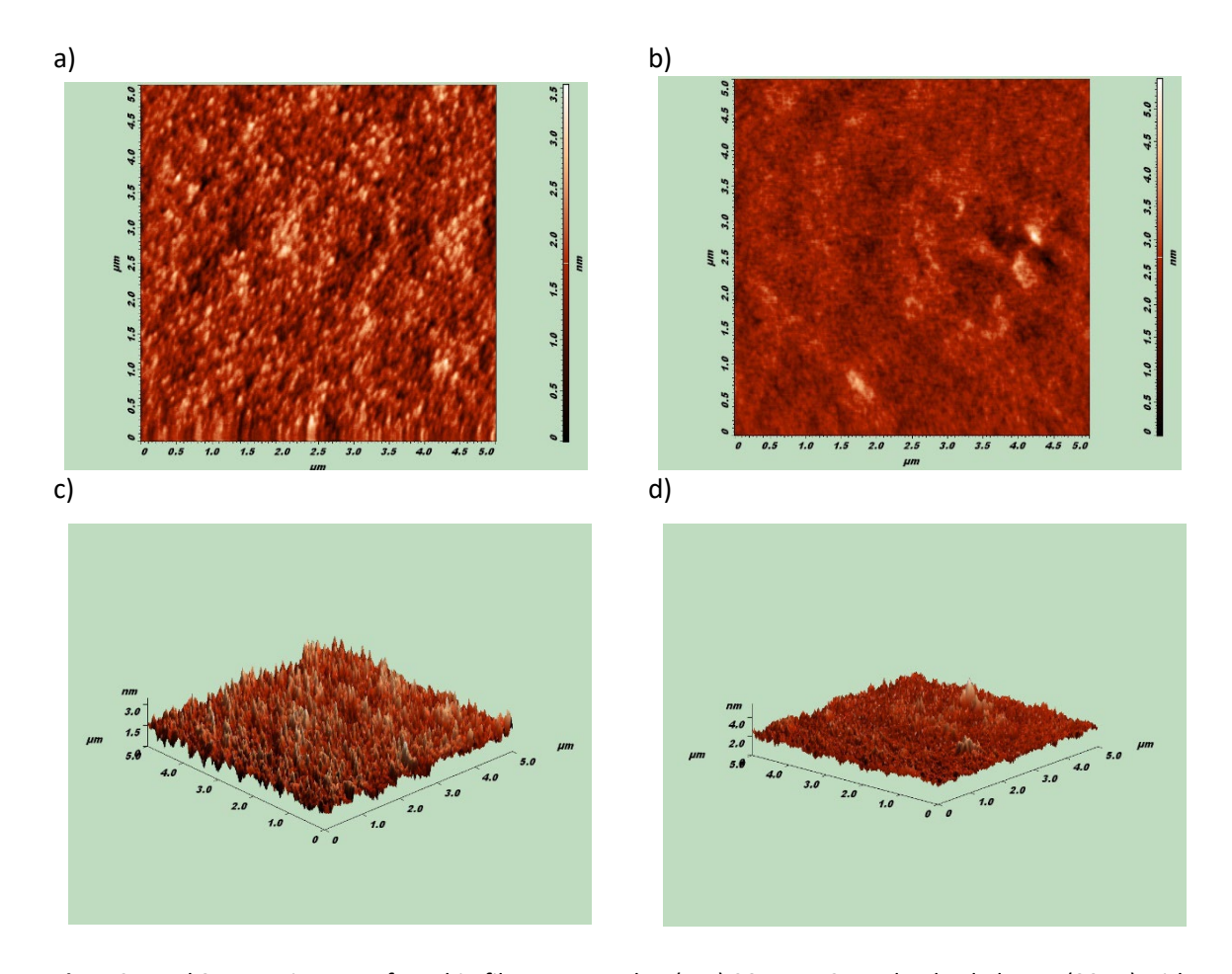
**Fig. 3** (a) Normalized J-V characteristics of encapsulated device with pulsed plasma at DC = 50% after fabrication and 2160 hours outside the glovebox. The variation of PCE (b) and FF (c) with time for encapsulated and non-encapsulated device.

Fig. 2a and Fig. 3a compare the performance of the best encapsulated devices based on continuous and pulsed plasma, respectively, over three months under ambient atmosphere. The stability of device with pulsed plasma encapsulation outperforms that based on continuous plasma coating. The higher stability of the device may prove that the pulsed plasma based encapsulation layer is more impervious (less permeable) to ambient oxygen than the CP-based counterpart. In addition to the low cost, sustainable preparation and fast synthesis of essential oils-based PP encapsulation layers, they are excellent candidates for OPVs and other optoelectronic devices. It should also be observed that the present encapsulation method does not cause any negative impact on the photovoltaic performance of the device as confirmed by Fig. S1. This can be attributed to the low RF power and short deposition time needed to produce these PP-thin film encapsulation layers.

To understand the properties of the synthesized PP-thin films and to investigate their potential for further applications, in particular in organic optoelectronics, a set of measurements was carried out which are discussed in the following sections.

## 3.2 Morphology and surface homogeneity of plasma polymerized thin films

The morphology features of the investigated thin films were studied using atomic force microscope (AFM). Fig. 4 shows the 2D and 3D images for PP-films deposited at 20 W continuous plasma and at DC of 50% pulsed plasma. Both samples show uniform and smooth surfaces with root mean square roughness of 0.38 nm and 0.42 nm for the pulsed and continuous plasma based polymers, respectively, which is in a good agreement with data in literature <sup>33, 42</sup>. Structural imperfections such as pinholes or dislocations within the encapsulation layer increase the permeation of oxygen and water molecules which negatively affects the device's stability <sup>43</sup>. Therefore, the defect-free morphology of PP-thin films is a promising feature that makes them excellent candidates as barrier layers for organic optoelectronic devices.



**Fig. 4** 2D and 3D AFM images of PP-thin films prepared at (a, c) 20 W RF CP and pulsed plasma (30 W) with DC of 50% (b, d).

The thickness of the investigated films was obtained by analyzing both reflection and transmission Ellipsometer data. The variation of film thickness over the substrate surface have shown a high degree of homogeneity as shown in Fig. 5. The values of film thickness ranged from 80 nm to 100 nm and from 200 nm to 300 nm for the pulsed and continuous plasma films, respectively. The average film thickness was found to increase from 78 nm to ~98 nm with increasing DC from 30% to 50% and remained almost the same (~96 nm) at DC of 70%. The thickness increases with duty cycle may be attributed to the increased probability of the polymerization reaction to the monomer vapour to occur with higher fraction of the deposition signal. In addition, all the films under investigations have shown high optical transmission exceeding 98% at a wavelength of 550 nm as displayed in Fig. S2.

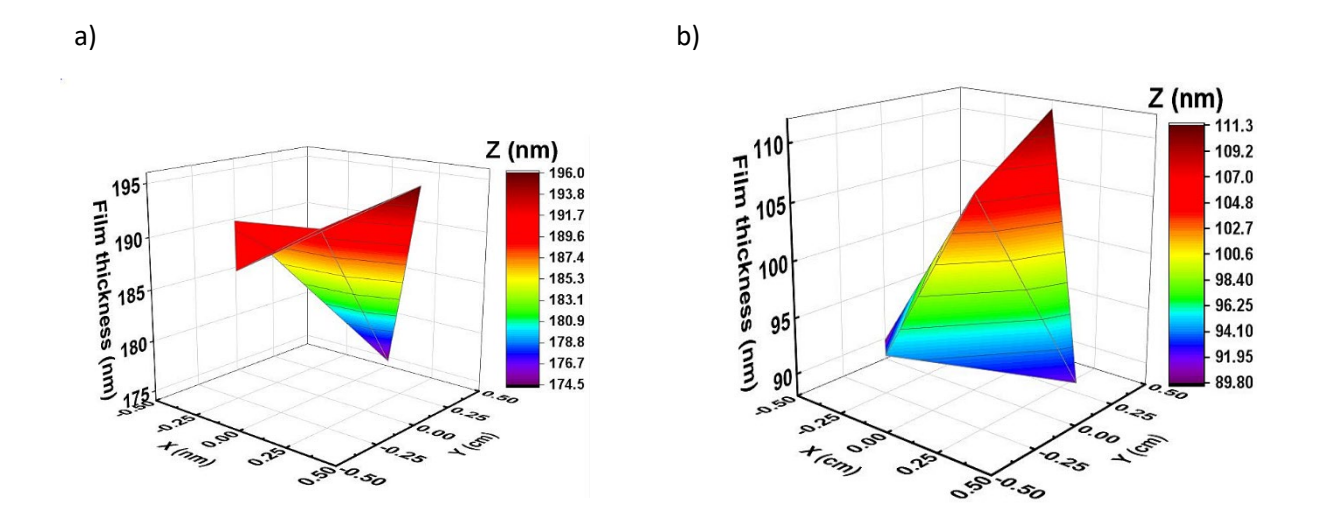


**Fig. 5** The variation of film thickness over the substrate surface, (a) CP at 20 W RF, (b) pulsed plasma at -DC 50%, measured by Ellipsometer.

## 3.3 Optical properties of PP-thin films

The high optical transmission of the investigated films is also confirmed by UV-VIS data as illustrated in Fig. 6, while the absorption spectrum of the monomer (Geranium oil) can be found in Fig. S3. All wavelengths >approx. 380 nm are totally transmitted through the film, while absorption is observed for shorter wavelengths. Fig. 6 shows the UV-VIS absorption spectra of the continuous and pulsed plasma polymer thin films prepared at different RF power and different duty cycles. These datasets were recorded for the as synthesized samples without any further treatment. Similar absorption spectra were observed for all samples with absorption peak between 270–280 nm which may be assigned to the  $\pi$ - $\pi$ \* transition <sup>44</sup>. The optical bandgap ( $E_g$ ) of the investigated films was determined using Tauc plots as shown in Fig. 6 (c &d ) according to the following equation:

$$\alpha h v = A \left( h v - E_g \right)^n \tag{1}$$

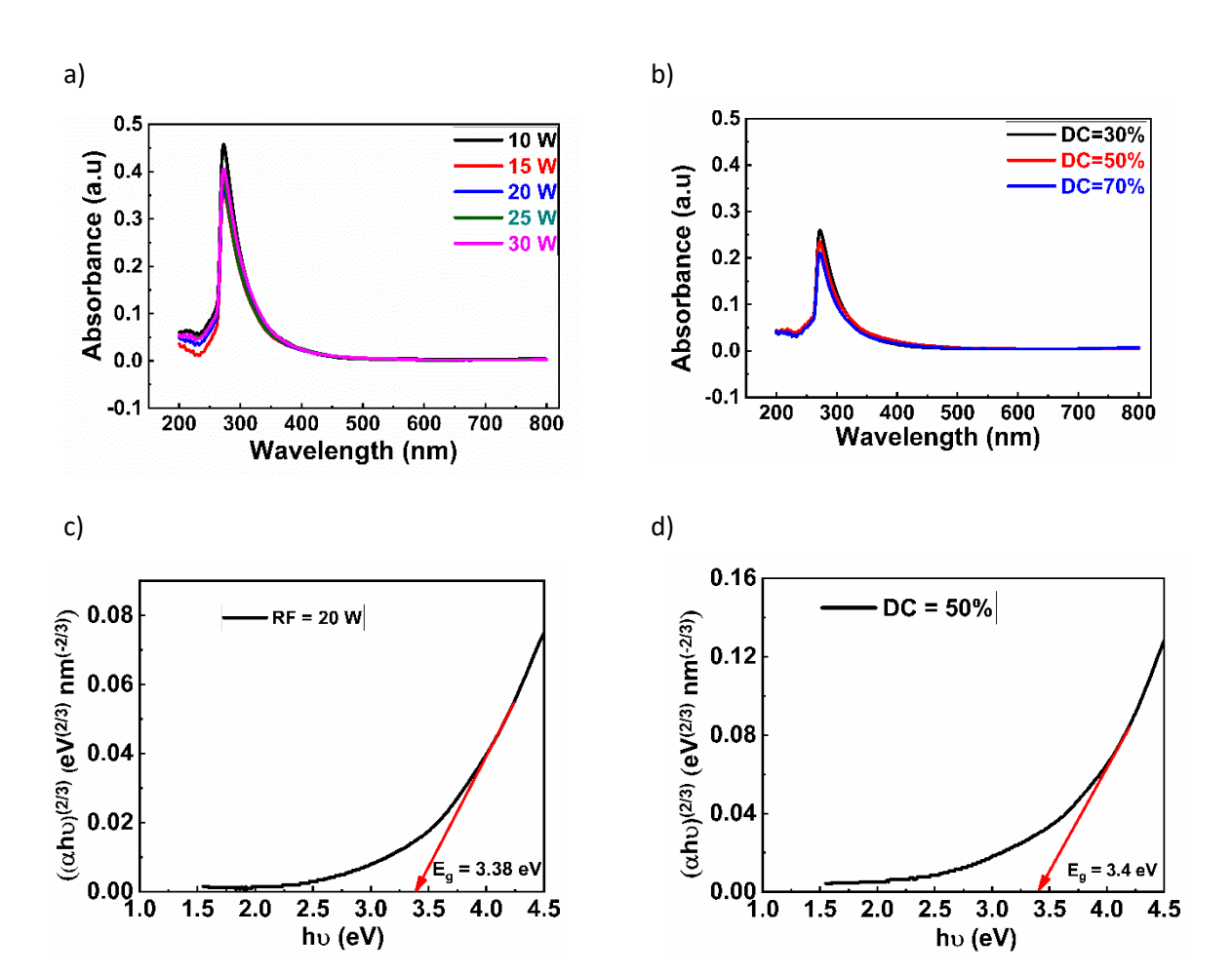
Where h is Planck's constant, A is an energy-independent constant, and  $\upsilon$  is the frequency of the incident light (Hz). The value of n depends on the distribution of the density of states and the transition mode, n can be 0.5 or 3/2 for direct allowed and forbidden transition, respectively, or 2 and 3 for indirect allowed and forbidden transitions, respectively <sup>35, 45</sup>. In this work, n of 3/2 was used for all the investigated PP-thin films as it gave the best linear fitting.  $\alpha$  is the absorption coefficient (cm<sup>-1</sup>) which can be related to the absorbance and the optical path within the material (film thickness, d) as <sup>46</sup>:

$$\alpha (cm^{-1}) = \frac{2.303 * Absorbance}{d (cm)}$$
 (2)

The values of optical bandgap for all the investigated films are listed in Table (1).

The ability of these plasma polymerized thin films to absorb light in the UV-range represents an added value to such materials in terms of their applicability as encapsulation layers for organic electronics. The absorption of these plasma polymers starts at almost 370 nm with an optical bandgap of (3.33-3.48 eV) which is in a good agreement with previously reported data <sup>42</sup>. It has been reported that the exposure of the different layers of OPVs, especially the photoactive layer, to high energy UV photons present in the solar spectrum is a determining factor to the overall device stability <sup>47</sup>.

Therefore, the prevention of such high energy photons from reaching the active layer of OPVs is crucial to reduce device degradation. Although glass substrates can absorb UV light with short wavelengths (<290 nm), these wavelengths are normally blocked by the Earth's atmosphere (Stratosphere layer) <sup>48</sup>. On the other hand, UV photons with longer wavelengths (UV-A and UV-B) which are present in natural sunlight reaching the Earth's surface are transmitted through glass substrates and can cause photo degradation of OPVs, (Fig. 6e). Therefore, the deposition of these PP films on the glass substrate represents a promising strategy to cut off destructive UV-light from the solar cell device, besides their application as physical encapsulation layers to the metal electrodes of OPVs and other organic electronics. As notable from Fig. 6 (a & b), the UV-absorbance of CP-based thin films is stronger than that of the pulsed plasma based counterparts which may be attributed to their larger absorption coefficient and thickness as confirmed by Ellipsometer data. Thus, film thickness can be adjusted to achieve the optimum UV absorption and hence, higher protection of the encapsulated device can be guaranteed without significant drop in the visible light reaching the photoactive layer due to the high transmission of these materials for visible wavelengths.



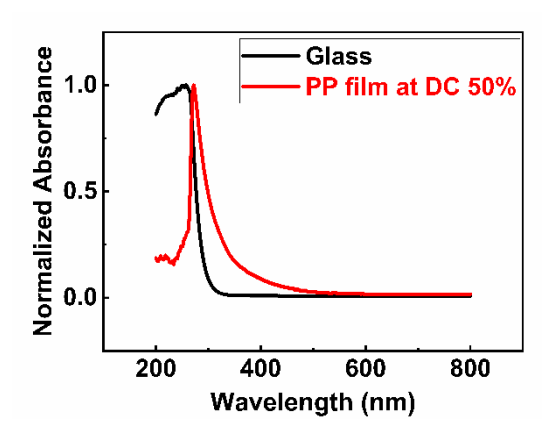


**Fig.6** UV-VIS spectra of the as prepared pp-thin films. (a) Continuous plasma. (b) Pulsed plasma polymer films. Tauc Plots for film polymerized at (c) RF = 20 W continuous plasma, (d) film deposited at RF = 30W pulsed plasma with duty cycle of 50%. (e): UV-VIS absorption of glass and a plasma polymer thin film deposited at RF = 30W pulsed plasma with DC of 50%, Y-axis was normalized to the maximum value to exclude the effect of thickness difference between the glass slide (1 mm) and that of the film (approx. 100 nm).

**Table 1** The optical bandgap Eg of different as-prepared PP-thin films.

Continuous plasma							
RF Power (W)	10	15	20	25	30		
Optical bandgap (eV)	<mark>3.45</mark>	<mark>3.42</mark>	<mark>3.38</mark>	<mark>3.44</mark>	<mark>3.33</mark>		
Pulsed plasma							
Duty cycle (%)	30		50		70		
Optical bandgap (eV)	<mark>3.33</mark>		<mark>3.4</mark>		<mark>3.42</mark>		

## 3.4 Chemical structure and photostability of PP-thin films

The chemical structure of the material is a key factor to understand its properties. The chemical composition of the precursor as well as the synthesized films was investigated by studying their FTIR spectra. Fig. 7a shows the FTIR spectrum of Pelargonium graveolens monomer, the band around 3370 cm<sup>-1</sup> represents the stretching OH of alcohol. The strong peak at 2940 cm<sup>-1</sup> with the two shoulders at 2870 and 2960 cm<sup>-1</sup> accounts for the different –C-H stretching vibrations <sup>49</sup>. The two peaks at 1712 cm<sup>-1</sup> and 1730 cm<sup>-1</sup> are assigned for C=O stretch of carbonyl compounds <sup>33</sup>, while the peaks at 1453 and 1377 cm $^{-1}$  are attributed to CH $_2$   $^{50}$  and CH $_3$   $^{51}$  bending vibrations, respectively. The weak peak at 1670 cm<sup>-1</sup> represents the C=C of alkenes <sup>42</sup>. The peak at 1057 and 1173 cm<sup>-1</sup> appear as a result of the C-O-C and C-OH stretching, respectively 50, 52. Similar FTIR spectra were obtained for both, continuous and pulsed plasma, in terms of peak positions, while the absorbance intensity of some peaks varied with varying deposition parameters. Fig.7 (b& c) shows the FTIR spectra for the synthesized films, the broad band around ~3400 cm<sup>-1</sup> is attributed to the O-H stretching vibration of alcohol groups. The peak at ~1707 cm<sup>-1</sup> refers to the stretching C=O of carbonyl groups. In case of continuous plasma polymers, two emerging peaks at wavenumbers of 1380 cm<sup>-1</sup> and 1457 cm<sup>-1</sup> are assigned to the C-H bending of CH3-and CH2-groups, respectively. Moreover, the emerging peak around 2960 cm<sup>-1</sup>, with the highest intensity at RF = 10W, is assigned to the C-H asymmetric stretching. In contrast, for pulsed PP-films, the presence of the peak at approx. 2960 cm<sup>-1</sup> can be observed, and

with low intensity, at DC of 50% and 70%, while the CH<sub>2</sub> and CH<sub>3</sub> related peaks completely disappeared. The disappearance of these bonds may be attributed to the high deposition power that can lead to the breakage of weak bonds within the monomer molecules during polymerisation reaction. The higher the deposition RF power, the higher the energy of the ions, electrons, and free radicals within the plasma reactor.

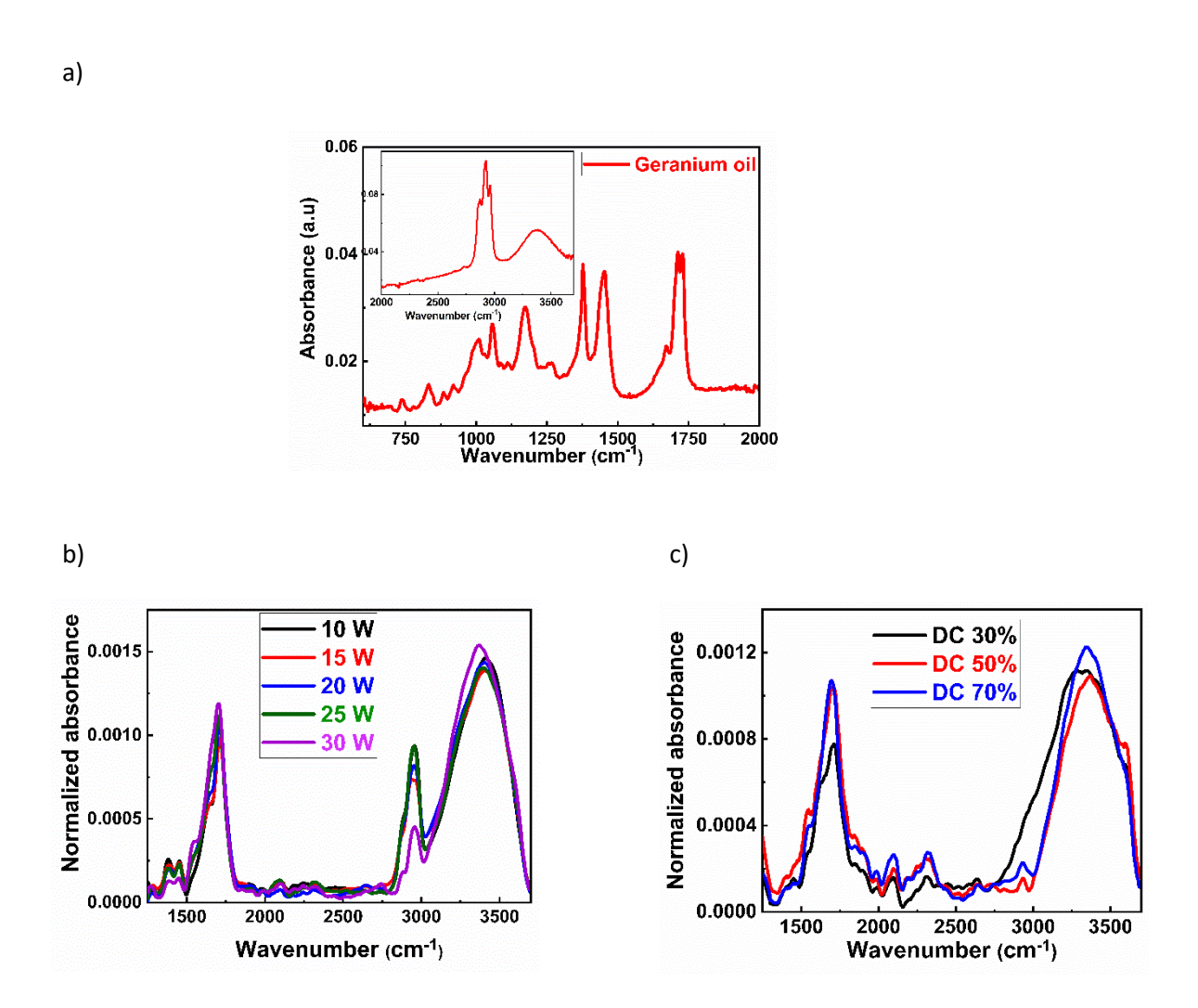
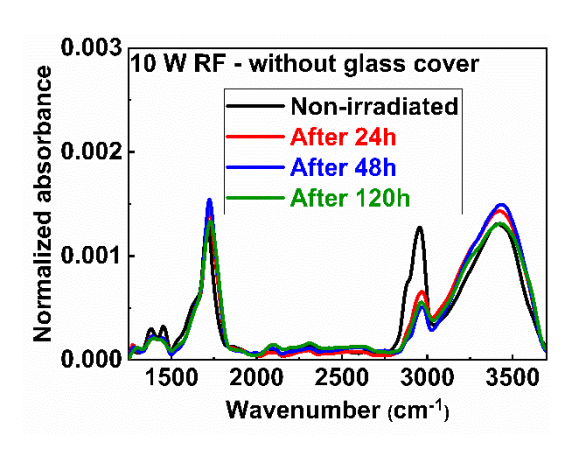


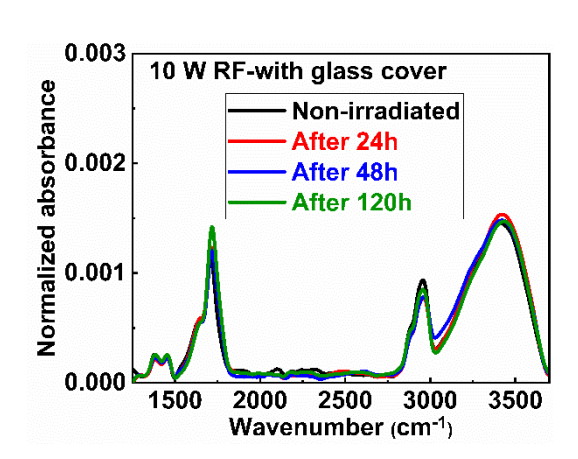
Fig. 7 FTIR spectra of (a) Geranium oil, (b) CP-based, and (c) pulsed plasma based polymer thin films.

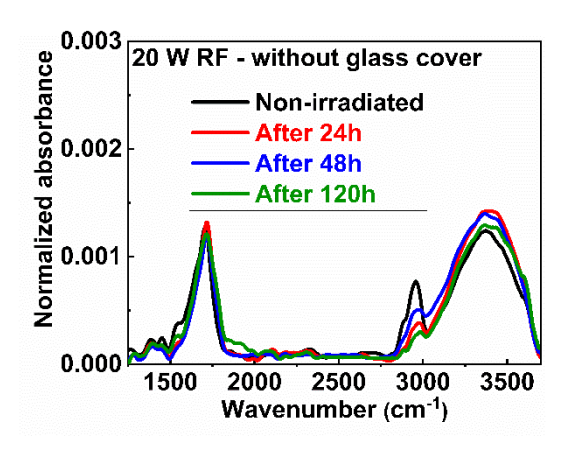
Due to the exposure of the encapsulation layers to incident solar light during device operation, it is important that the encapsulation material possesses a high degree of photostability. In this work, the stability of both continuous and pulsed plasma polymerized films were investigated against UV-B ( $\lambda$ =300±25 nm) radiation. The films were exposed directly to UV radiation for 24, 48 and 120 hours and their stability was evaluated through variations of their FTIR spectra. UV-irradiation can result in structural changes within the plasma polymerized thin films depending on the energy of radiation and exposure time. To exclude the effect of unnatural wavelengths (<300 nm), the irradiated films were covered by a glass petridish which is transparent to wavelengths >300 nm (see Fig. S4 - Fig. S6). Upon exposure to UV-B, both continuous and pulsed plasma based films started to show slight changes in their FTIR spectra compared to the non-irradiated counterparts. The response of the investigated PP-films varied with their preparation conditions. The resulting changes in the corresponding FTIR spectra of the irradiated samples are represented by an increase or decrease in the intensity of the different

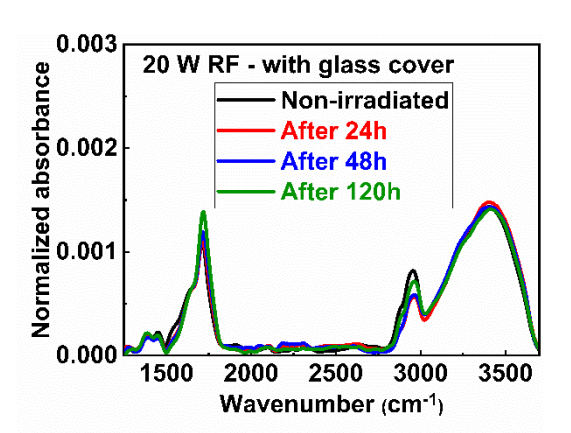
peaks. In order to exclude the influence of film thickness on peak intensity, absorption data were normalized over the total area under the curve for the range of interest in the FTIR spectrum.

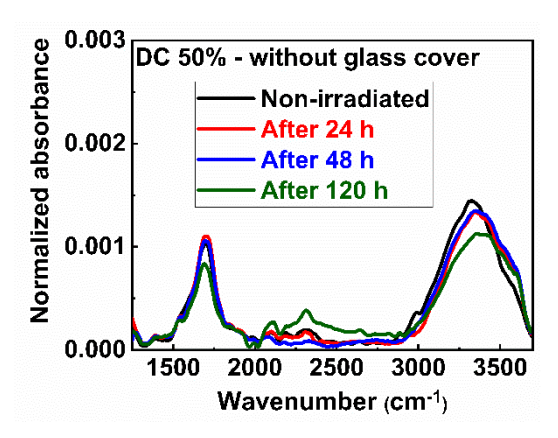
For both continuous and pulsed plasma based films, it can be observed from Fig. 8 that the change in the intensity of the absorbance peaks is minor especially when using the glass cover. For the films deposited at continuous RF power, the stretching C-H vibration around 2900 cm<sup>-1</sup> was mainly affected, particularly when unnatural high energy photons were included (without glass cover). The change is higher in case of low deposition RF power which may be attributed to the presence of residual monomer on the film's surface due to incomplete polymerisation. The decrease of the C-H vibration band (around 2900 cm<sup>-1</sup>) is accompanied by an increase in the intensity of C=O and OH peaks which can be ascribed to photo oxidation reaction upon UV exposure. Pulsed plasma-based thin films have shown higher stability as almost no changes in their FTIR spectra have been observed, even after 120 hours of UV-B exposure when glass cover was used. In addition, minor changes were found even when high energetic UV photons were present. These were visible as a decrease in the intensity of C=O vibration band with a simultaneous broadening in the OH vibration peak, which increased with exposure time. This behaviour may be attributed to the conversion of carbonyl (C=O) into carboxyl (COOH) groups in the presence of molecular oxygen.

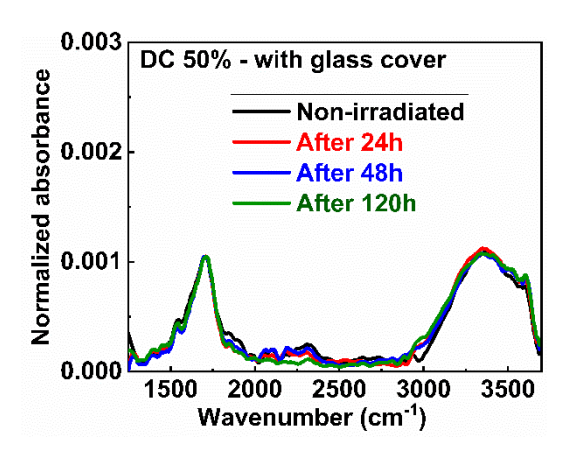








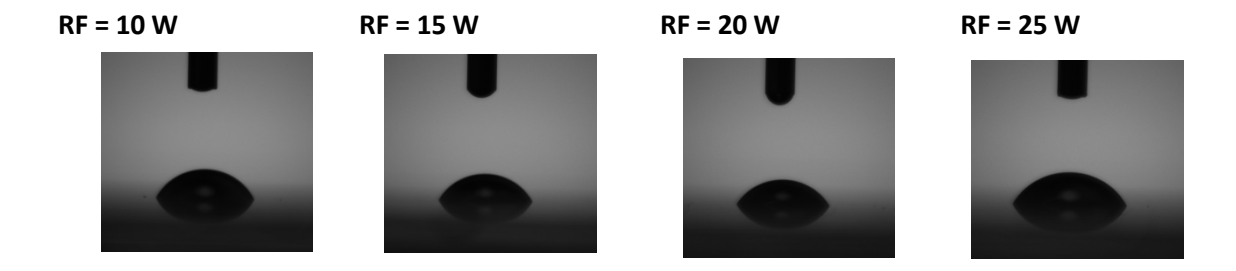




**Fig. 8** The variation of FTIR spectra of the CP and pulsed plasma based polymer thin films with UV-B irradiation without (left) and with (right) glass cover for variable irradiation time.

## 3.5 Water contact angle of PP-thin films

The water contact angle (WCA) is an important parameter for encapsulation materials. The hydrophobicity of an organic material is significantly improved by the presence of non-polar CH groups. Fig. 9 shows the water contact angles of all the investigated plasma polymer thin films. Films based on continuous plasma have much higher WCA than those based on pulsed plasma as summarized in Table (2). In case of continuous PP-films, the relatively high WCA (compared to pulsed PP-films) can be attributed to the presence of more non-polar groups such as CH2 and CH3, as confirmed by their FTIR spectra (Fig. 7). The value of WCA of the sample prepared at 30 W is somewhat lower than those of other samples deposited in continuous power mode. This variation can be linked to the weaker presence of non-polar groups with respect to polar groups (C=O and OH). It is noteworthy to mention that an efficient encapsulation material should possess large water contact angles so that it can provide higher protection to the photovoltaic device, especially in high humidity or even rainy conditions, on large scale applications. From Fig. 2 and Fig. 3, OPVs encapsulated with pulsed plasma -based thin films have higher stability in ambient conditions than those based on continuous plasma. On the other hand, WCA measurements revealed that CP-based thin films are more hydrophobic than the pulsed plasma-based counterparts. Therefore, the deposition of a CPbased thin layer on the top of the encapsulation layer synthesized with pulsed plasma can be more protective approach to OPVs in humidified or rainy weather. This bilayer encapsulation can be carried out in the same procedure as the single layer deposition without any considerable excess cost.



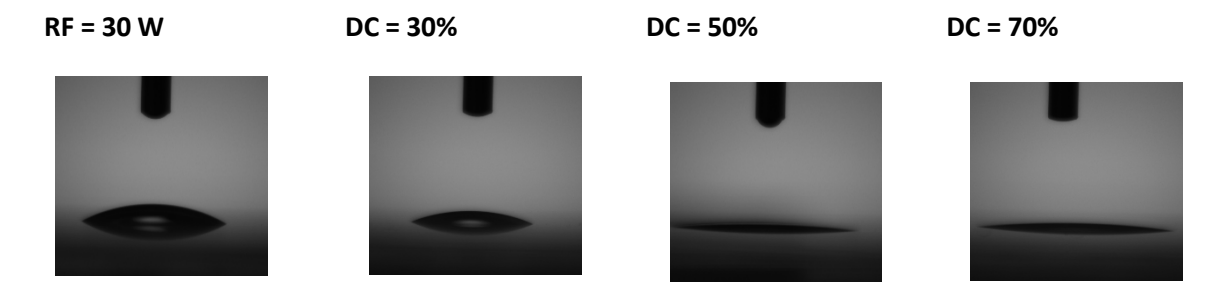


Fig. 9 Water contact angle for the as-synthesized plasma polymer thin films on glass substrates.

Table 2 Values of water contact angle for the different as-prepared PP-thin films.

Continuous plasma							
RF Power (W)	10	15	20	25	30		
Water contact angle (°)	64.01	60.48	58.05	60.56	29.31		
Pulsed plasma							
Duty cycle (%)	30		50		70		
Water contact angle (°)	22.38		4.47		8.55		

#### 4. Conclusion

Efficient encapsulation layers for organic photovoltaic (OPV) devices were prepared using time- and cost-effective RF plasma polymerization of Pelargonium graveolens. The low RF deposition power coupled with room temperature fabrication of these polymer thin films does not cause any damage to the layers of the device during encapsulation. The dry (solvent-free) deposition of these plasma polymers in addition to their dielectric nature and high adhesion results in an effective contact with the metal electrode without influencing the photovoltaic parameters of the device. Both continuous and pulsed plasma-based polymers have enhanced the device stability with an optimum performance for films deposited at a pulsed plasma of 30 W and duty cycle of 50%. The best encapsulated device retained two thirds (66%) of its initial power conversion efficiency and 87% of its fill factor without any change in the open circuit voltage after three months in ambient atmosphere, while the reference device degraded within the first month. More interestingly, the encapsulated device was found to keep > 57% of PCE after more than 4.5 months. In addition, the synthesized films have shown high stability under UV-B irradiation. The sustainability and time- and cost-effectiveness of this method make it a promising candidate for large scale encapsulation of OPVs and other organic optoelectronic devices, especially for flexible ones.

#### **Conflicts of interest**

The authors declare no conflict of interest

## Acknowledgement

Michael S. A. Kamel would like to acknowledge the financial support by the college of Science and Engineering, James Cook University (JCU), Townsville, Australia through JCUPRS scholarship.

## References

- 1. H. Liu, M. Li, H. Wu, J. Wang, Z. Ma and Z. Tang, *Journal of Materials Chemistry A*, 2021, **9**, 19770-19777.
- 2. D. He, F. Zhao, L. Jiang and C. Wang, *Journal of Materials Chemistry A*, 2018, **6**, 8839-8854.
- 3. Y. Chang, X. Zhu, K. Lu and Z. Wei, Journal of Materials Chemistry A, 2021, 9, 3125-3150.
- 4. X. Dong, P. Shi, L. Sun, J. Li, F. Qin, S. Xiong, T. Liu, X. Jiang and Y. Zhou, *Journal of Materials Chemistry A*, 2019, **7**, 1989-1995.
- 5. K. Liu, T. T. Larsen-Olsen, Y. Lin, M. Beliatis, E. Bundgaard, M. Jørgensen, F. C. Krebs and X. Zhan, *Journal of Materials Chemistry A*, 2016, **4**, 1044-1051.
- 6. S. Jeong, B. Park, S. Hong, S. Kim, J. Kim, S. Kwon, J.-H. Lee, M. S. Lee, J. C. Park, H. Kang and K. Lee, ACS Applied Materials & Interfaces, 2020, 12, 41877-41885.
- 7. Y. Lin, B. Adilbekova, Y. Firdaus, E. Yengel, H. Faber, M. Sajjad, X. Zheng, E. Yarali, A. Seitkhan, O. M. Bakr, A. El-Labban, U. Schwingenschlögl, V. Tung, I. McCulloch, F. Laquai and T. D. Anthopoulos, *Advanced Materials*, 2019, **31**, 1902965.
- 8. M. Kaltenbrunner, M. S. White, E. D. Głowacki, T. Sekitani, T. Someya, N. S. Sariciftci and S. Bauer, *Nature communications*, 2012, **3**, 1-7.
- 9. Y. Liu, N. Qi, T. Song, M. Jia, Z. Xia, Z. Yuan, W. Yuan, K.-Q. Zhang and B. Sun, *ACS Applied Materials & Interfaces*, 2014, **6**, 20670-20675.
- 10. J. Zhao, Y. Li, G. Yang, K. Jiang, H. Lin, H. Ade, W. Ma and H. Yan, *Nature Energy*, 2016, **1**, 15027.
- 11. N. Grossiord, J. M. Kroon, R. Andriessen and P. W. Blom, *Organic Electronics*, 2012, **13**, 432-456.
- 12. Y. Liang, Z. Xu, J. Xia, S. T. Tsai, Y. Wu, G. Li, C. Ray and L. Yu, *Advanced Materials*, 2010, **22**, E135-E138.
- 13. Q. Liu, Y. Jiang, K. Jin, J. Qin, J. Xu, W. Li, J. Xiong, J. Liu, Z. Xiao, K. Sun, S. Yang, X. Zhang and L. Ding, *Science Bulletin*, 2020, **65**, 272-275.
- 14. C. Li, J. Zhou, J. Song, J. Xu, H. Zhang, X. Zhang, J. Guo, L. Zhu, D. Wei and G. Han, *Nature Energy*, 2021, **6**, 605-613.
- 15. M.-A. Pan, T.-K. Lau, Y. Tang, Y.-C. Wu, T. Liu, K. Li, M.-C. Chen, X. Lu, W. Ma and C. Zhan, *Journal of Materials Chemistry A*, 2019, **7**, 20713-20722.
- 16. Y. Cui, H. Yao, J. Zhang, T. Zhang, Y. Wang, L. Hong, K. Xian, B. Xu, S. Zhang and J. Peng, *Nature communications*, 2019, **10**, 2515.
- 17. L. Meng, Y. Zhang, X. Wan, C. Li, X. Zhang, Y. Wang, X. Ke, Z. Xiao, L. Ding, R. Xia, H.-L. Yip, Y. Cao and Y. Chen, *Science*, 2018, **361**, 1094-1098.
- 18. Z. N. Jiang, B. Gholamkhass and P. Servati, *JOURNAL OF MATERIALS RESEARCH*, 2019, **34**, 2407-2415.
- 19. A. Uddin, M. B. Upama, H. Yi and L. Duan, *Coatings*, 2019, **9**, 65.
- 20. A. Kovrov, M. Helgesen, C. Boeffel, S. Kröpke and R. R. Søndergaard, *Solar Energy Materials and Solar Cells*, 2020, **204**, 110210.
- 21. K. Kawano, R. Pacios, D. Poplavskyy, J. Nelson, D. D. C. Bradley and J. R. Durrant, *Solar Energy Materials and Solar Cells*, 2006, **90**, 3520-3530.
- 22. H. Neugebauer, C. Brabec, J. C. Hummelen and N. S. Sariciftci, *Solar Energy Materials and Solar Cells*, 2000, **61**, 35-42.
- 23. I. Litzov and C. J. Brabec, *Materials*, 2013, **6**, 5796-5820.
- 24. S. Lattante, *Electronics*, 2014, **3**, 132-164.
- 25. M. De Jong, L. Van Ijzendoorn and M. De Voigt, Applied Physics Letters, 2000, 77, 2255-2257.
- 26. Y.-H. Kim, S.-H. Lee, J. Noh and S.-H. Han, *Thin Solid Films*, 2006, **510**, 305-310.
- 27. J. Ahmad, K. Bazaka, L. J. Anderson, R. D. White and M. V. Jacob, *Renewable and Sustainable Energy Reviews*, 2013, **27**, 104-117.
- 28. G. Dennler, C. Lungenschmied, H. Neugebauer, N. S. Sariciftci, M. Latreche, G. Czeremuszkin and M. R. Wertheimer, *Thin Solid Films*, 2006, **511**, 349-353.

- 29. M. H. Park, J. Y. Kim, T. H. Han, T. S. Kim, H. Kim and T. W. Lee, *Advanced Materials*, 2015, **27**, 4308-4314.
- 30. H.-K. Seo, M.-H. Park, Y.-H. Kim, S.-J. Kwon, S.-H. Jeong and T.-W. Lee, *ACS applied materials & interfaces*, 2016, **8**, 14725-14731.
- 31. H. C. Weerasinghe, Y. Dkhissi, A. D. Scully, R. A. Caruso and Y.-B. Cheng, *Nano Energy*, 2015, **18**, 118-125.
- 32. F. Li and M. Liu, *Journal of Materials Chemistry A*, 2017, **5**, 15447-15459.
- 33. K. Bazaka, J. Ahmad, M. Oelgemöller, A. Uddin and M. V. Jacob, *Scientific reports*, 2017, **7**, 1-9.
- 34. M. V. Jacob, N. S. Olsen, L. J. Anderson, K. Bazaka and R. A. Shanks, *Thin Solid Films*, 2013, **546**, 167-170.
- 35. J. Ahmad, K. Bazaka and M. V. Jacob, *Electronics*, 2014, **3**, 266-281.
- 36. K. Bazaka, M. V. Jacob and B. F. Bowden, Journal of Materials Research, 2011, 26, 1018-1025.
- 37. K. Bazaka, M. V. Jacob and K. Ostrikov, *Chemical reviews*, 2016, **116**, 163-214.
- 38. K. Bazaka, M. V. Jacob, R. J. Crawford and E. P. Ivanova, *Acta biomaterialia*, 2011, **7**, 2015-2028.
- 39. K. Bazaka and M. V. Jacob, *Electronics*, 2013, **2**, 1-34.
- 40. M. B. Upama, M. Wright, N. K. Elumalai, M. A. Mahmud, D. Wang, K. H. Chan, C. Xu, F. Haque and A. Uddin, *Current Applied Physics*, 2017, **17**, 298-305.
- 41. M. B. Upama, N. K. Elumalai, M. A. Mahmud, C. Xu, D. Wang, M. Wright and A. Uddin, *Solar Energy Materials and Solar Cells*, 2018, **187**, 273-282.
- 42. A. Al-Jumaili, K. Bazaka and M. V. Jacob, *Nanomaterials*, 2017, **7**, 270.
- 43. V. I. Madogni, B. Kounouhéwa, A. Akpo, M. Agbomahéna, S. A. Hounkpatin and C. N. Awanou, *Chemical Physics Letters*, 2015, **640**, 201-214.
- 44. C. D. Easton and M. V. Jacob, *Thin Solid Films*, 2009, **517**, 4402-4407.
- 45. Z. Z. You and G. J. Hua, *Vacuum*, 2009, **83**, 984-988.
- 46. R. Dewi, 2020.
- 47. J. B. Patel, P. Tiwana, N. Seidler, G. E. Morse, O. R. Lozman, M. B. Johnston and L. M. Herz, *ACS Applied Materials & Interfaces*, 2019, **11**, 21543-21551.
- 48. E. Yousif and R. Haddad, SpringerPlus, 2013, 2, 398.
- 49. J. Ahmad, K. Bazaka, M. Oelgemöller and M. V. Jacob, *Coatings*, 2014, 4, 527-552.
- 50. A. B. D. Nandiyanto, R. Oktiani and R. Ragadhita, *Indonesian Journal of Science and Technology*, 2019, **4**, 97-118.
- 51. S.-Y. Lin, W.-T. Cheng, Y.-S. Wei and H.-L. Lin, *Polymer journal*, 2011, **43**, 577-580.
- 52. H. Fabian, M. Jackson, L. Murphy, P. H. Watson, I. Fichtner and H. H. Mantsch, *Biospectroscopy*, 1995, **1**, 37-45.